ESTIMATION OF COUNT AND MASS OF CITRUS FRUIT DROP USING MACHINE VISION

By

DAEUN CHOI

A THESIS PRESENTED TO THE GRADUATE SCHOOL
OF THE UNIVERSITY OF FLORIDA IN PARTIAL FULFILLMENT
OF THE REQUIREMENTS FOR THE DEGREE OF
MASTER OF SCIENCE

UNIVERSITY OF FLORIDA

2013

To my family and love, for all their support

ACKNOWLEDGMENTS

I would like to express my sincere gratitude to all of the people that have helped me to accomplish during my master's program. It has been a challenging yet amazing experience during the study. It would not be possible if I did not have support from people around me. First and foremost, I would like to thank my advisor Dr. Won Suk Lee for providing me a chance to pursue my graduate studies, also for his guidance and support throughout my research and thesis. I would like to thank to my supervisory committee members, Dr. Reza Ehsani and Dr. Fritz Roka for their advices.

I also would like to express my appreciation for having amazing lab mates and for their amazing ideas shared with me. I really enjoyed our conversations and discussions all the time. I am thankful for Mr. Zingaro as well for helping me to finish my hardware design.

Lastly, I would like to express my deepest appreciation to my parents, and fiancé for always loving me and believing in me. I cannot imagine how hard it would be without them by my side.

TABLE OF CONTENTS

Page

LIST OF TABLES

LIST OF FIGURES

Abstract of Thesis Presented to the Graduate School
of the University of Florida in Partial Fulfillment of the
Requirements for the Degree of Master of Science

ESTIMATION OF COUNT AND MASS OF CITRUS FRUIT DROP
USING MACHINE VISION

By

Daeun Choi

December 2013

Chair: Won Suk “Daniel” Lee
Major: Agricultural and Biological Engineering

A machine vision system for estimating citrus fruit drop count and its mass was developed. The objectives were to design rugged hardware for outdoor imaging, to develop an image processing algorithm to estimate count and mass of the citrus fruit drop and to create a geo-referenced fruit drop map.

Image acquisition hardware was developed to be used in a commercial citrus grove specifically for outdoor imaging conditions. The image processing algorithm included normalization of illumination, citrus detection using a logistic regression classifier, and least square circle fitting for estimating size and mass of the citrus.

Performances of the machine vision algorithm were analyzed using two different criteria. Firstly, capability of detecting citrus without any missed fruit which was denoted as accuracy was analyzed. The accuracy varied in experiment trials, and the highest accuracy was 89 percent while the lowest was 59 percent. The second criterion was analysis of false positives which represented incorrect detection of background objects as citrus. The percentage of false positives also varied between the trials, the highest error was 30 percent and the lowest error was 2.6 percent.

Result of the experiments showed that each area in citrus groves had different count and mass of the citrus drop. This is because each area in fields had different site-specific variable factors such as nutrient levels, soil pH, diseases such as citrus greening, canopy size etc. Among those factors, the result showed that especially spraying CMNP before harvesting caused significant drop. However, CMNP sprayed for past couple of years did not have specific effect on citrus drop.

CHAPTER 1
INTRODUCTION

Citrus fruit is one of valuable crops in agricultural and international fruit markets. The consumption of citrus has exhibited world-wide growth since the late 19th century. Citrus fruit can be produced only in particular areas in the world due to the geographical and climate reasons. The most significant amount of citrus production is from certain countries such as the United States, Brazil and countries near the Mediterranean. The United States was the second largest producer in 2012 with a total of 8.2 million tons, which amounts to 15% of the total world citrus production. In the United States, the state of Florida is the largest citrus producer. According to the United States Department of Agriculture (USDA) – National Agricultural Statistics Services (NASS), 146 million boxes of citrus were produced in 2011-2012 in Florida (Figure 1-1) which supported 71 percent of the entire production in the United States.

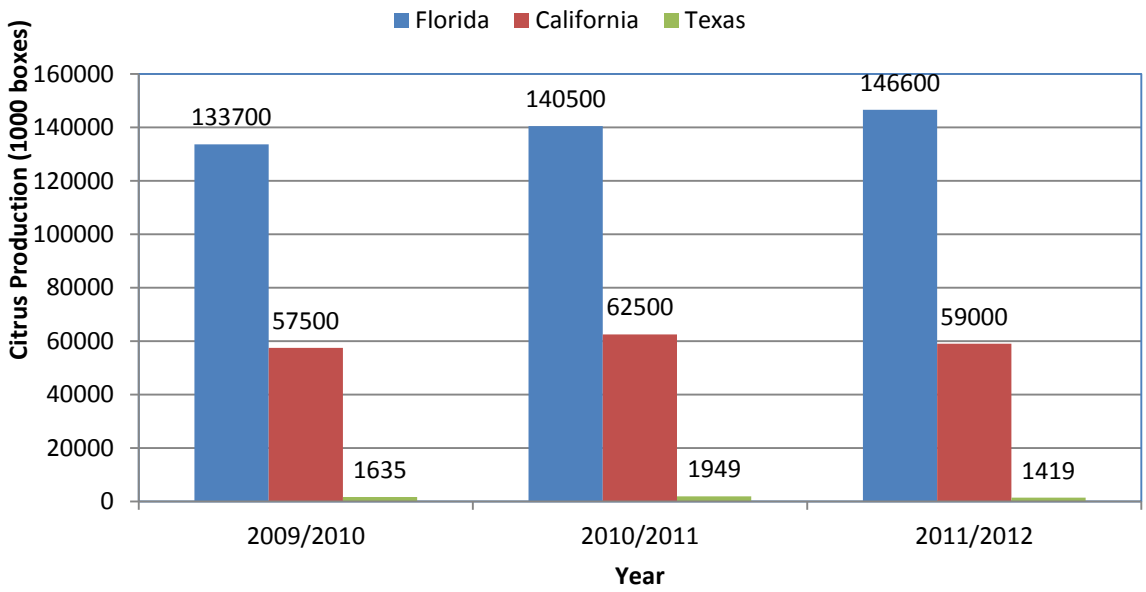

Figure 1-1. Citrus production in Florida, California and Texas states (USDA-NASS, 2013)

Citrus Greening Disease (HLB)

Huanglongbing (HLB) which is an exotic disease in citrus, also called citrus greening, has spread in an extremely rapid manner. This disease often causes small, bitter taste and improper colored fruit. Additionally, HLB is considered one of main reason of early citrus fruit drop which consequently decreases the production. Table 1-1 illustrates the decrease in estimated production for a 2012/2013 season. In October in 2012, the USDA expected 74 million boxes of non-Valencia orange and 80 million boxes of Valencia oranges to be produced in Florida. However, mostly because of early citrus fruit drop from a bad combination of the HLB and unfavorable weather, estimated production dropped to 67 million boxes of non-Valencia and 71 million boxes of Valencia in April, 2013.

Table 1-1. Florida 2012/2013 Estimated Production Drop (Unit: thousand Boxes, USDA-NASS, 2013).

	October	April
Non-Valencia	74000	67000
Valencia	80000	71000
All Oranges	154000	138000

To facilitate management of the HLB for growers in citrus groves and anticipate change in future production, evaluating how many and where the early fruit drop is occurring is an important task. In other words, estimation of the amount of yield decrease resulting from early citrus fruit drop in specific location would help the citrus growers so that citrus growers can manage the disease efficiently. Once the accurate estimation of the fruit is obtained, efficient management of the HLB can be achieved by creating a geo-referenced fruit drop map which is one of major concepts in precision agriculture.

Precision Agriculture

Precision agriculture which is also called site-specific crop management is the management of inputs for crop production in site-specific way (John Deere, 2010).

Under the site-specific management, each zone is treated differently corresponding to its characteristic. This characteristic includes soil nutrient, amount of yield, soil pH, diseases, moisture contents, etc. The first step of implementing precision agriculture is creating an in-field spatial variability map. The spatial variability map can be created using Geographic Information System (GIS). Based on characteristics of each zone, Variable Rate Technology (VRT) system distributes inputs according to in-field spatial variability of different factors incorporated with a GPS receiver so that the crop can be grown in an optimal condition.

Mechanical Harvesting

About 93 percent of citrus are harvested manually. Manual harvesting involves a significant labor and time. In an effort to reduce costs of harvesting, mechanical citrus harvesting has been implemented as an alternative.

One of the mechanical harvester, continuous canopy shake and catch harvesters are shown in Figure 1-2. A couple of canopy shakers works at the same time, each of them shakes a bed and swell sides of the canopy simultaneously. The harvested fruit were caught in a catch frame. To evaluate performance of the mechanical harvester, count and mass of citrus fruit harvested by the mechanical harvester should be measured. However, the canopy shakers could not catch all the harvested fruit since there was a gap between two catch frames allowing the fruits to fall down to the ground. To obtain an accurate estimate of the efficiency of the mechanical harvester, count and mass of the dropped fruit on the ground also need to be counted.

Figure 1-2. Canopy shakers and catch frame.

Additionally, to make mechanical harvesting more efficient, a chemical compound, 5-chloro-3-methyl-4-nitro-1H-pyrazole (CMNP), was developed to remove fruit with less force. However, the CMNP has a downfall causing significant amount of early fruit drop from trees before harvesting. In order to identify effect of spraying CMNP, estimation of the amount of early citrus fruit drop is also important.

Machine vision

Due to huge production areas, manual estimation of the citrus fruit drop is considered as a time consuming and labor intensive task. Automation of fruit drop count and mass estimation can be accomplished using machine vision. Machine vision is a tool consisting of imaging devices and processors for automatic visual inspection such as surveillance, vehicle guidance, process control etc. Machine vision can also provide accurate information for precision agriculture in many applications such as sorting fruit and yield estimation (Yang et al., 2012) and disease detection (Li et al., 2013, Pourreza et al, 2013).

Thesis Objective

Overall goal of this research was to develop an automation system for identifying count and mass of citrus fruit drop using machine vision.

Additionally, specific objectives were as follows.

1. To build a rugged hardware system for image acquisition in a citrus grove,
2. To develop a machine vision algorithm that will successfully estimate the number of citrus fruit along with their mass, and
3. To create spatial variability map for citrus fruit drop.

These objectives will benefit citrus growers for several reasons such as,

1. To identify efficiency of citrus mechanical harvesters, and
2. To analyze an impact of CMNP or HLB in early fruit drop.

Related Literatures

Citrus Detection and Counting Algorithm

Annamalai and Lee (2003) developed a citrus yield mapping system using machine vision. The objective was to develop a machine vision system for detecting citrus and to count citrus fruit in images to provide an estimated yield map effectively. The algorithm dealt two types of images: close view images containing 2 or 3 oranges and normal view images including 8 to 10 oranges. The algorithm consisted of thresholding in a Hue-Saturation plane and counting citrus pixels. The coefficient of determination (R^2) was equal to 0.76 between manual counting of citrus in the images and counting by the algorithm. The source of errors was citrus fruit occluded by leaves.

Also, Annamalai and Lee (2004) developed a real-time system for estimation of citrus yields. The algorithm was developed in a similar way to a study reported in 2003. However, the R^2 value was 0.42 between counts by the algorithm and actual harvested

citrus and 0.53 between yield production model developed in this study and actual data. They pointed out that errors were from a limited number of cameras. Another source of error was counting method for overlapped citrus. The algorithm could not count the citrus when more than 3 fruits were overlapped.

Patel et al. (2012) suggested automatic segmentation for yield estimation of various fruit such as citrus, apple, pomegranate, peach, and plum using color and shape. Images were acquired in RGB color space and then were transformed into the Lab color space. Color information of 'a' component plane that were used to detect fruit region. Circle fitting was performed to find fruits in the images. However, the average error in validation set was high (31%) since small oranges were not detected by the algorithm.

Various Fruit Detection Algorithm

Stajnko et al. (2003) developed a method to estimate the number of apple and its size in an orchard. Thermal images of temperature gradient between fruit and background was used. For fruit detection algorithm, simple thresholding was conducted in RGB color space and a normalized difference index (NDI). The coefficient of determination (R^2) ranged from 0.83 to 0.88 between manually counted number and estimation by the algorithm. An apple's longest segment were used to estimate mass. Based on the longest segment measurement, a diameter was estimated by multiplying it to the pixel/mm proportion. For the diameter estimation, R^2 ranged between 0.68 and 0.70.

Another apple detection and counting algorithm was developed by Zhao et al. (2005). An algorithm to detect apple fruit on trees was developed. A stereo vision was used to acquire images with accurate apple position. Redness was used to differentiate

apples from background. Texture analysis was also applied to find edges which were combined with the redness. After detection, circle fitting was performed to find the position of the apples in images.

Ling et al. (2004) detected mature tomato in grayscale images obtained from dividing R component by G component in RGB color space. By this method, different illumination conditions were removed. Ridler's adaptive segmentation method was used to detect mature tomatoes. Edges were found by chain code technique then Circular Hough Transform (CHT) and chord construction were applied to find center location of the tomatoes. Result from chord construction algorithm was less accurate than CHT. However, chord construction was faster and more suitable for real-time system.

Chi et al. (2004) developed chord reconstruction algorithm for detecting tomatoes by circle finding. This algorithm was developed for robotic harvesters. The result was compared with circular Hough Transform (CHT). The chord reconstruction was more suitable for real-time system since the processing time was much faster than CHT. Also, the algorithm was able to detect occluded tomatoes. However, the chord reconstruction method had less accuracy than CHT.

Yang et al. (2007) developed color segmentation (CLG) method to detect tomatoes in images. The CLG method was based on color structure code (CSC) which links or connects regions according to similarity of color. In CLG, a group of pixels which were called island grew or connected if color distance between same-level islands was within threshold. After growing, islands which were under threshold size were discarded and the rest of them was considered as tomato objects.

Citrus Mass Estimation Algorithm

Chinchuluun et al. (2009) developed a machine vision system to identify citrus fruit and its size on a canopy shaker and catch harvester. An image acquisition system was developed and the system was mounted on a canopy shaker and a catch harvester. Citrus detection and size identification algorithm was developed using a Bayesian classifier. Firstly, color information was collected in Hue, Saturation and Intensity (HSI) color space and YIQ (Luma and Chrominance) color space. After fruit pixels were detected, watershed segmentation was implemented and a total area of citrus fruit was measured. R^2 was 0.962 between actual weight and the sum of the total citrus fruit area. R^2 value between actual weight and the sum of fruit diameter was 0.963 and R^2 value between citrus fruit count and actual weight was 0.892.

Shin et al. (2012) developed a system for postharvest citrus mass estimation. For citrus detection, color information in Hue, Saturation and Intensity (HSI) color space and luminance, chrominance in blue and chrominance in red (YCbCr) color space was used. Logistic regression method was used for a classifier. During segmentation, high-saturation-pixels on fruit area were recovered by highly saturated area recovering algorithm (HSAR). Watershed algorithm using H-minima transform was used to segment connected fruit in order to identify the number of fruit and fruit sizes.

Comparison of the Research in the Thesis and Related Articles

The studies by Chinchuluun et al. (2009) and Shin at al. (2012) are similar with this research in terms of objectives which were citrus fruit detection and mass estimation. Images in introduced studies were taken in an enclosed box so that the field of view was narrower and illumination condition was under control. However, this research dealt with outdoor imaging which had extremely varying illumination condition

and wide field of view. Since colors of objects in images varied significantly in non-uniform illumination conditions, more sophisticated and reliable algorithm towards illumination condition was developed for this research.

Studies by Annamalai and Lee (2003, 2004), Patel at al. (2012), Stajnko et al. (2003), and Zhao et al. (2005) were conducted in outdoor conditions. The images were acquired with close and narrow field of view so that the fruits size was relatively large to be detected. However, experiments in this study dealt with distant citrus fruits in images so the size of fruits was very small. Additionally, images included more complicated the background containing many objects such as soil, grass and irrigation pipe.

CHAPTER 2
MATERIALS AND METHODS

Image Acquisition

Hardware

The machine vision system consisted of two parts. In this chapter, the image acquisition equipment and camera-triggering device are illustrated. The machine vision system had two color CCD cameras with a microprocessor, two VGA monitors, metal mounting frames for vehicle and an encoder.

The cameras that were used were smart cameras (NI-1772C, National Instruments Corporation, Austin TX), which contained its own microprocessor (1.6 GHz, Intel Atom). The cameras had a 1/3” CCD sensor to generate regular RGB color images. The camera was designed to withstand harsh condition which was the main reasons for being used in this study. The majority of industrial cameras were designed for indoor applications which would result in failure when used in outdoor situations.

This study required acquiring images in commercial citrus grove whose environmental situation made image acquisition a tough task because of sandy, dusty and wet conditions.

Figure 2-1 (A) shows a frontal view of the camera. A metal shield was installed on the top of the cameras to protect from tree branches and dew. Figure 2-1 (B) illustrates side view of camera mounted on pan and tilt frame. The camera had three connection lines to a terminal block, VGA/USB and Ethernet. The terminal block had eight isolated input/output channels and power supply.

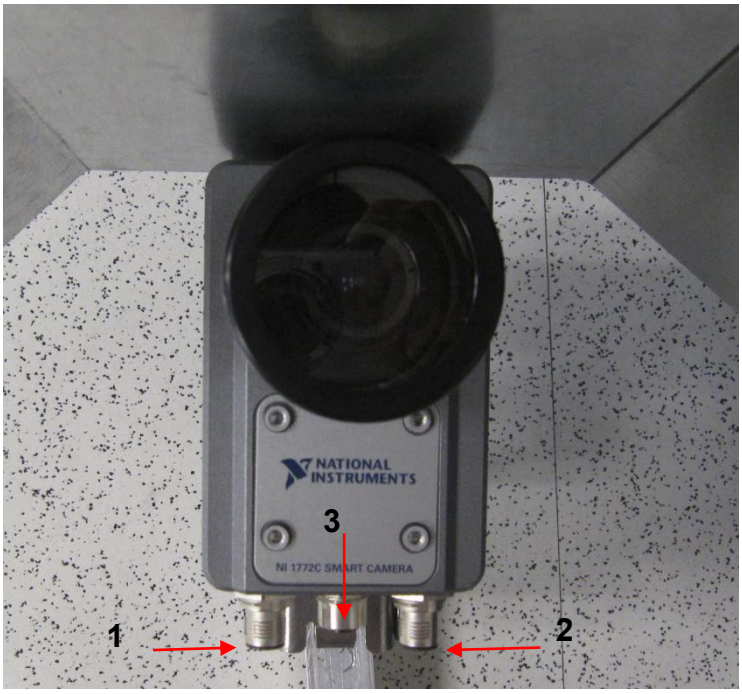

A

B

Figure 2-1. Figure Camera used in the experiment (NI 1772C Smart Camera, National Instrument Corporation). A) front side of camera with protection shield on top and connection lines (1. Terminal block, 2: Gigabit Ethernet, 3.USB/VGA). B) Side view of camera mounted on the pan and tilt frame. Photo courtesy of author, Daeun Choi.

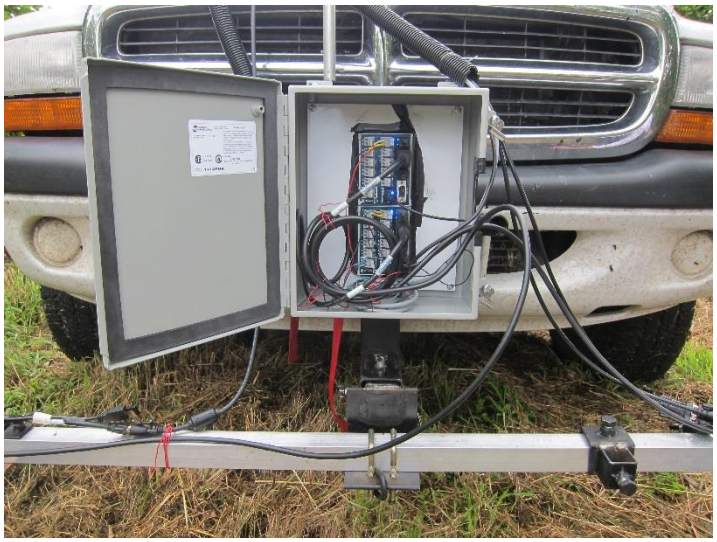

A

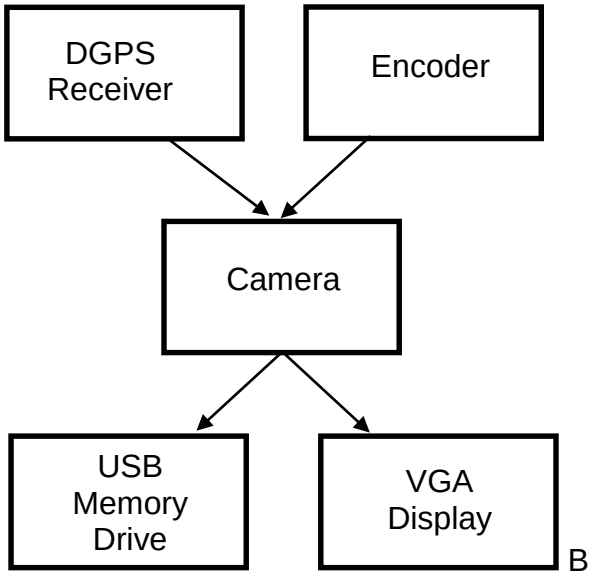

B

Figure 2-2. Input and output of cameras. A) Terminal block of the cameras attached on the mounting frame. B) Schematic flow chart of input and output of camera.

These three lines were in charge of transferring and saving of data during the experiment. Digital data from an encoder and GPS were transmitted to the camera through the terminal block shown in Figure 2-2 (A). Figure 2-2 (B) shows schematic diagram of input and output data connection of cameras. The encoder was used as an external triggering device which helped avoid overlapped areas between images. The

type of encoder used here was an incremental rotary encoder which generated digital pulses (0 and 1) when its shaft rotated. The encoder was attached to a small tire located at the back of a truck where the camera was installed (Figure 2-3). The images were acquired every 0.9 m since the shortest horizontal field of view of an image was approximately 0.9 m.

When image acquisition was triggered, a GGA sentence from a DGPS receiver was saved for time and position where an image was taken. Images and GPS information were saved in an USB memory drives inserted in the cameras which were used for creating a geo-referenced fruit drop map. Communication between the camera and the receiver was through industrial RS-232 serial port.

Figure 2-3. Encoder attached on a small tire on the back side of truck. Photo courtesy of author, Daeun Choi.

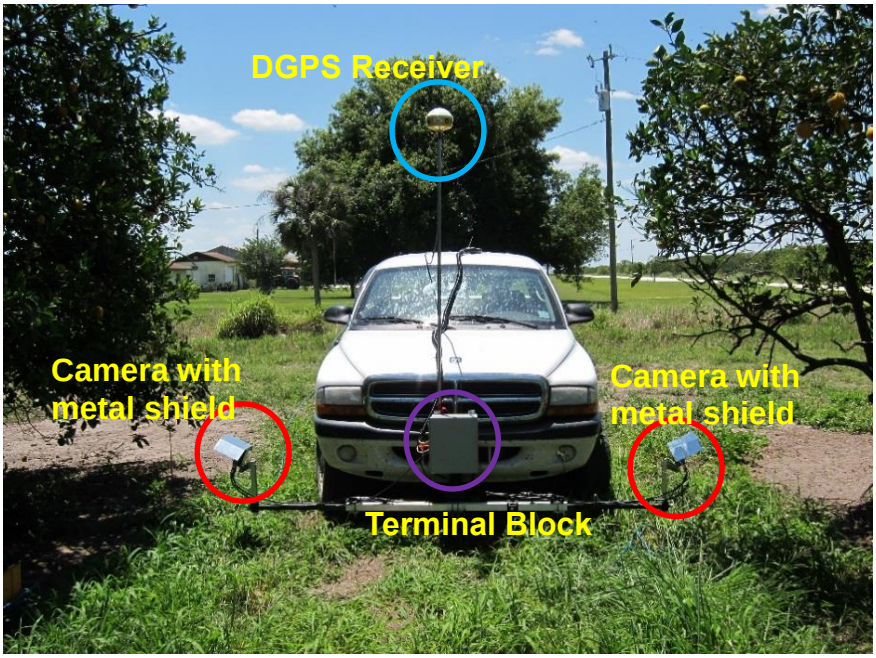

Figure 2-4. Final hardware setup. A DGPS receiver and two cameras attached to the mounting frame. Red circle: camera with metal shield, purple circle: terminal block and light blue circle: DGPS receiver. Photo courtesy of author, Daeun Choi.

Figure 2-4 shows final hardware setup used in the experiments. Two cameras were installed on both side of the truck at 0.5 m above from the ground. Also, a DGPS receiver was installed along with the camera.

Image Acquisition Software

The camera had a microprocessor and a real-time operating system was installed. An executable software for image acquisition was developed using LabVIEW 2012 (National Instrument Corporation, Austin TX). This image acquisition software developed as a graphical user interface (GUI) shown in Figure 2-5 had three main purposes: displaying an image, indicating digital input from the encoder, and displaying position information from the DGPS receiver. If digital pulse was detected, a green status light illuminated to inform the user. In an input box, the number of pulses from the encoder was displayed. If the number of pulses reached the specified number, the

software triggered the camera to acquire an image. Also, baud rate was able to be adjusted in the software for RS-232 communication to DGPS receiver. Position information sent from the DGPS receiver was displayed in front panel.

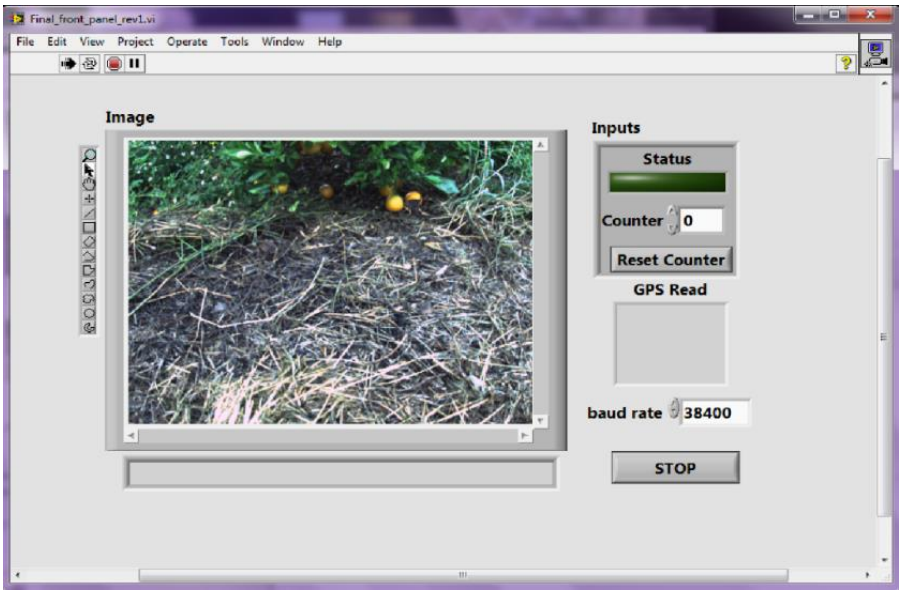

Figure 2-5. Front panel of image acquisition software. This software includes image display, input status and GPS coordinate indicator.

Field Experiment

The detection and counting algorithm of citrus fruit was developed using images from several field experiments in Duda & Sons grove (Immokalee, FL), and Lykes Bros. Inc. grove (Ft. Basinger, FL). The average row spacing for three citrus groves was 7.3 m and tree spacing was 4.6 m. Since dropped citrus fruit was an object of interest in the experiments, images covered wide area of the ground, especially under the canopy. The clearance between the ground and the lowest canopy for hand harvested rows at the Duda grove was less than 30 cm. While this would not be a problem for hand harvesting, it turned to be troublesome for image acquisition with prototype system developed in this study. For the mechanical harvested rows at the Lykes grove, the

canopy was skirted in order to make it accessible by a mechanical harvester and so the lowest canopy was about 46 cm from the ground (Figure 2-6).

Figure 2-6. View of skirted canopy in commercial citrus grove for mechanical harvesting and dropped fruit due to the disease and CMNP. Photo courtesy of author, Daeun Choi.

Field experiments were conducted in various situations during hand and mechanical harvesting. For the hand harvesting, multiple crews picked up citrus fruits on the trees manually. Each crew had a bag for the harvested citrus and after filling up the bag, the crews transferred fruits to the tub shown in Figure 2-7. The harvested fruit in the tubs were then collected by goat truck shown in Figure 2-8.

Figure 2-7. Tub for Hand Harvesting. Photo courtesy of author, Daeun Choi.

Figure 2-8. Goat truck. Photo courtesy of author, Daeun Choi.

Machine Vision Algorithm

After acquiring images, machine vision algorithm largely consisted of five steps: image normalization, classification, texture analysis, fitting circles, estimate fruit count and mass. Image normalization was applied in order to remove the effect of varying illumination conditions. Then a logistic regression classifier was used in classification. Also, entropy values were calculated to remove incorrectly detected background from the classification. After detection, circle was fitted to measure diameter and position for estimating mass of dropped fruit in images.

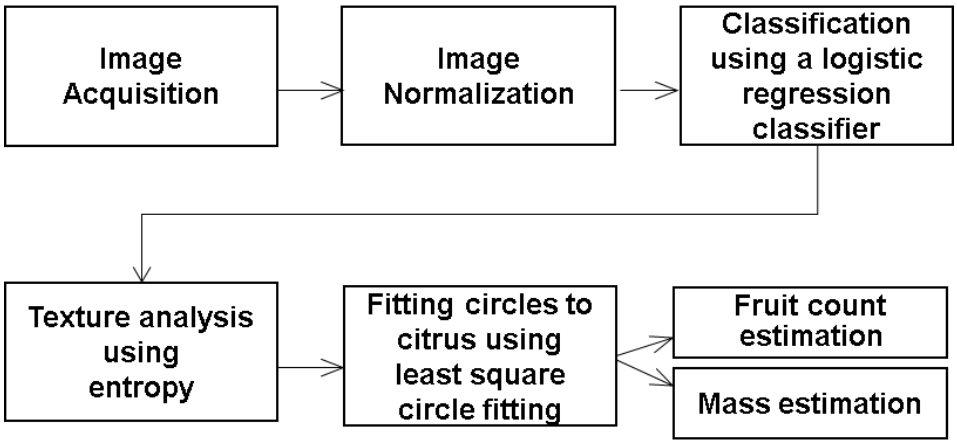

Figure 2-9. Flow chart of machine vision algorithm.

Image Used in Algorithm

A total of 1470 images was used in the experiments. Each image's resolution was 480 by 640. A pixel located in the first top and left can be expressed as I (1, 1) where I means the image matrix. The resolution represents the quality of an image. Figure 2-10 shows a comparison of high resolution and low resolution images. Figure 2-10 (A) shows an image of low resolution while Figure 2-10 (B) has high resolution which has more clear view of objects with more details.


A


B

Figure 2-10. Image quality comparison. A) 640×480. B) 3648×2736. Photo courtesy of author, Daeun Choi.

The resolution of image was chosen to be 480 × 640 to allow faster processing time. Although low resolution images processed images faster, it required the algorithm to be more precise since objects in the images had less pixels than in the high quality images.

RGB Color Space and Intensity

After acquiring images, images were saved in a USB drive in BMP format. The images were represented in regular RGB color space which is one of three color channel representation models. The R channel means red image, G means green image and B means Blue color image. Each channel has an 8-bit depth value which

ranges from 0 to 255 (=2^8). A full color image refers to a composite image of the red, green and blue image which has depth of 24-bits through the combination of 8-bit 3-channel values. All values of R, G, B channel can be represented in a normalized format in range of [0, 1] for the convenience (Equation 2-1).

$$\begin{bmatrix} \bar{R} \\ \bar{G} \\ \bar{B} \end{bmatrix} = \begin{bmatrix} R/255 \\ G/255 \\ B/255 \end{bmatrix} \quad (2\text{-}1)$$

Among original RGB images, 10% of images were randomly chosen to be a training set and the rest of the images was assigned as a validation set. The training set was used to collect the color and size information of objects. To obtain RGB color information for each object, the image pixels were classified to four classes based on the objects found in the training set. Four classes were 1. citrus, 2. leaf, 3. dead leaf, twig and tree, and 4. soil. Each object in the training set was manually cropped and analyzed. The color information was analyzed in the RGB color space and converted into other color spaces such as: 1) hue, saturation, and value (HSV), 2) luminance, blue-difference chroma, and red-difference chroma (YCbCr), 3) lightness, a and b color-opponent dimensions (Lab), 4) luma and chrominances (YIQ). The conversion formulation are illustrated in later part of this chapter.

Figure 2-11 shows histograms of R, G and B components in RGB color space. In Figure 2-11 (A), the citrus class had R component values ranging from 50 to 255. Although the average of R component for a Leaf, dead leaf, twig, tree and soil was relatively lower than citrus, the entire area of citrus ranging from 50 to 255 was overlapped with other classes.

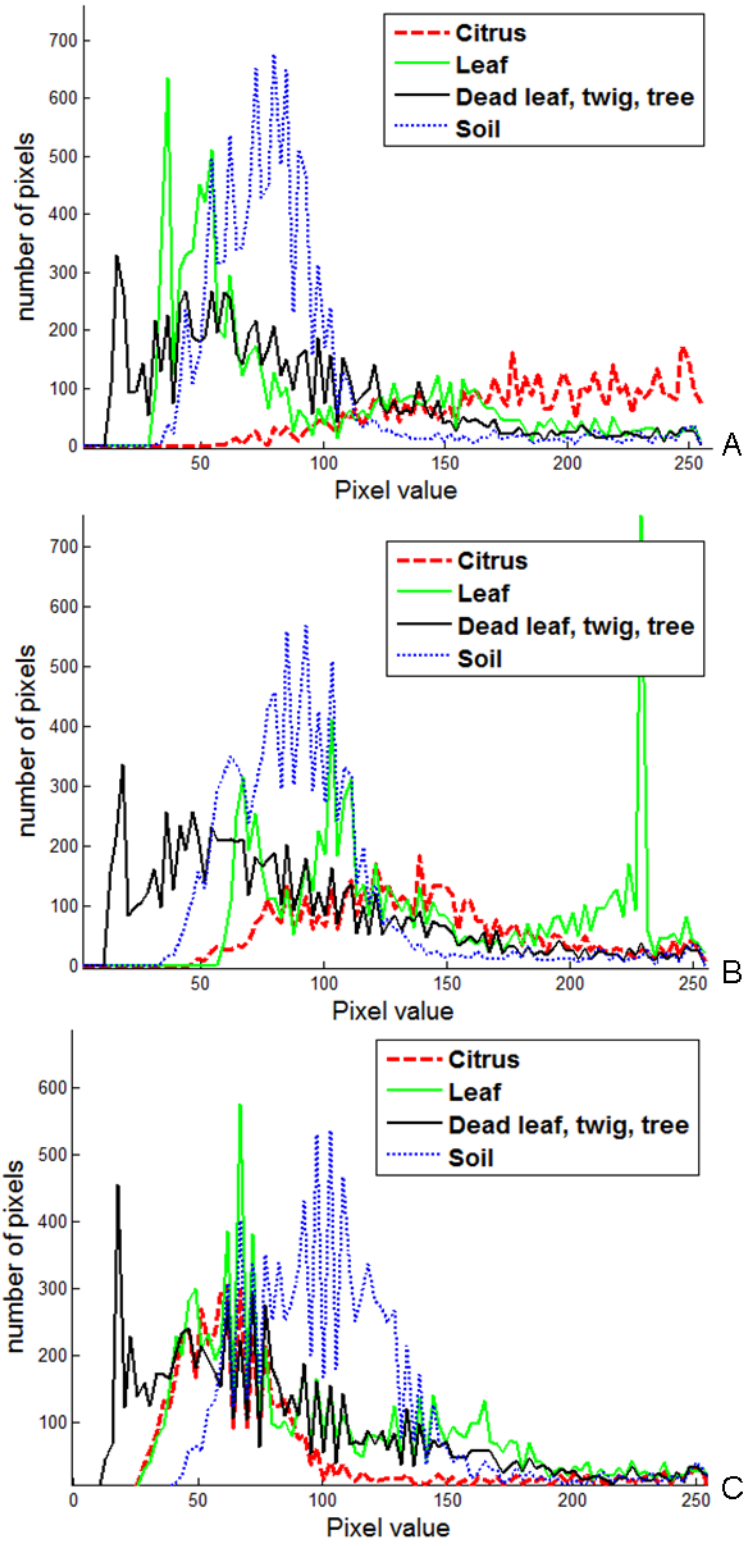

Figure 2-11. Histogram of R, G and B component (A, B and C, respectively): citrus, leaf, dead leaf, twig, tree and soil. Each class is overlapped and share similar color value

Likewies, the citrus class was placed in mid range overlapping most of the area with other classes in the histogram of G component in Figure 2-11 (B). In B component in Figure 2-11 (C), all classes had lower pixel values, and overlapped each other. This overlapping area means all the classes shared similar color values with each other. One of the main reason of wide overlapping area among the classes was the different illumination conditions of the images.

The images were taken in outdoor condition in the citrus grove under direct sunlight. Illumination was not controllable which caused the most critical problem for image processing. In this study, illumination was defined using intensity which refers to the amount of the light in a pixel. The intensity can be defined in various forms, but here, intensity was calculated by Equation 3-2 (ITU, 1995).

$$I = 0.2989R + 0.5870G + 0.1140B \quad (2\text{-}2)$$

In Equation 2-2, R, G, and B represent the values of each component in the RGB color space. The definition in Equation 3-2 is the same definition as the Y component value in both YIQ and YCbCr color spaces. Using the intensity, an average illumination of the image was calculated by an average value of the intensity.

The illumination condition in the training set was divided into three classes based on illumination conditions: low, mid and high illumination. The intensity values ranged 0-115, 115-164, and 164-255 for the low, mid and high illumination classes, respectively.

The varying illumination caused dramatic change in color values in the images. For example, the citrus in high illumination conditions had the color similar to yellow and the citrus under low illumination had a brown color.

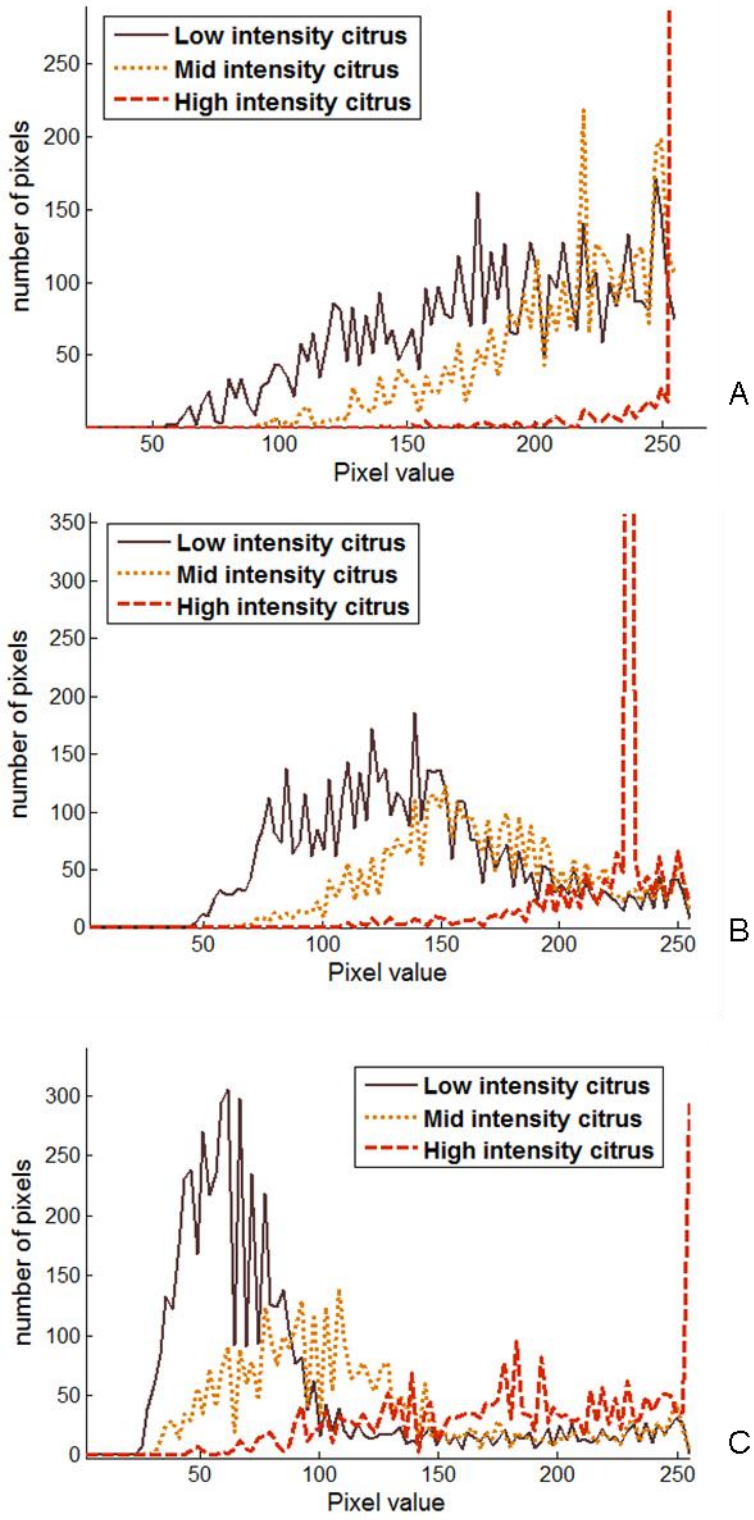

Figure 2-12. Color variation in R, G, and B components (A, B and C, respectively) according to different average intensity values.

Figure 2-12 (A). and (B) display the color variation in the citrus class according to their illumination conditions. Depending on the illumination, the range of each component value varied. Especially in G and B components in Figure 2-12 (B) and (C) demonstrate the signigicant differences in color among the low, mid and high illumination classes. In Figure 2-12, the 4 classes: citrus, leaf, dead leaf and soil were all overlapped by other objects in the histogram. On top of that, the different illumination conditions of the images increased the range of overlapping which made even more difficult to identify citrus fruit from the background. These extended overlapped areas in histogram added difficulties in classification of objects.

Normalization of illumination

Additionally, the illumination condition changed significantly even within an image. This was because the images covered a wide range of area (0.9 m horizontally and 2.1 m vertically) which included the ground under the canopy. Figure 2-13 shows one of example images used in the experiments. The ground had shadows in some areas, which made the color of objects darker. In contrast, the area without shadow resulted in the soil having an excessive amount of white color due to the high intensity.

This varying condition made segmentation complex because multiple segmentation models were required according to illumination levels. Although different segmentation methods could be applied depending on the illumination levels, it was not easy to make correct classification because the citrus pixels usually contained a higher intensity value than other pixels such as soil and twig. In other words, the citrus in the middle illumination condition had a higher intensity value than soil or twig pixels in high illumination condition.

Figure 2-13. Example image of varying illumination. Under the shadow objects were likely to have darker color and without the shadow, the pixels had high intensity.

Therefore, a process for removing the effect of illumination condition was required. In this study, normalization of illumination was proposed to relieve drastic changes in intensity level. Normalization of illumination is defined as Equation 2-3.

$$\begin{pmatrix} R' \\ G' \\ B' \end{pmatrix} = 255 \cdot \begin{pmatrix} R/I \\ G/I \\ B/I \end{pmatrix} \tag{2-3}$$

where $I = 0.2989R + 0.5870G + 0.1140B$.

By Equation 2-3, the effect of different illumination was removed and normalized. Dividing each component value by intensity, the coefficient for the R, G and B component values per unit intensity was obtained. Multiplying 255 made each class more distinguishable from other classes by increasing color difference. In Figure 2-13, the citrus fruit had yellow color in the high intensity area and dark orange color in the shadow area.

Figure 2-14. Normalization of illumination. Citrus fruit under different illumination conditions has similar color value compared to Figure 2-13.

However, in Figure 2-14, the intensity level throughout the image became approximately uniform so the citrus fruits had identical yellow color rather than different colors depending on the illumination. This process helped citrus fruit to be segmented more easily from other background objects. Table 2-1 shows RGB color values of each object in normalized image. By normalization, citrus had distinctive value (255, 255, 0) from other objects such as green, cyan and white color.

Table 2-1. RGB values of citrus, leaf, dead leaf and soil in normalized image.

	Citrus (Yellow)	High intensity leaf (Green)	Leaf and soil, dead leaf (Cyan)	Highly saturated area (White)
R	255	0	0	255
G	255	255	255	255
B	0	0	255	255

Conversion to H'S'V' and Y'Cb'Cr' Color Space

Normalized images were converted into Hue, Saturation and Value (HSV) color space and Luminance, blue-difference and red-difference Chroma components (YCbCr)

color space. For a regular RGB color image, the conversion formula is defined in Equation 2-4, 2-5, 2-6 (Gonzalez, 2008).

$$H = \begin{cases} \theta & if\ B \le G \\ 360 - \theta & if\ B > G \end{cases}, \quad \text{where, } \theta = \cos^{-1}\left[\frac{\frac{1}{2}(2R-G-B)}{\sqrt{(R-G)^2+(R-B)(G-B)}}\right] \tag{2-4}$$

$$S = 1 - \frac{3}{R+G+B}\min(R,G,B) \tag{2-5}$$

$$V = \frac{1}{3}(R+G+B) \tag{2-6}$$

To convert RGB color space to HSV color space, normalized RGB values ranging [0, 1] were used. Note that normalized RGB value and normalization of illumination (R'G'B') values are different in this study. With normalization of illumination values, H', S', and V' component values are defined as Equation 2-7, 8 and 9.

$$H' = \begin{cases} \theta & if\ B' \le G' \\ 360 - \theta & if\ B' > G' \end{cases}, \quad \text{where } \theta = \cos^{-1}\left[\frac{\frac{1}{2}(2R'-G'-B')}{\sqrt{(R'-G')^2+(R'-B')(G'-B')}}\right], \tag{2-7}$$

$$S' = 1 - \frac{3}{R'+G'+B'}\min(R',G',B'), \tag{2-8}$$

$$V' = \frac{1}{3}(R'+G'+B') \tag{2-9}$$

H and H' values range [0, 360], S and S', V and V' values can have [0, 1]. Also, RGB to YCbCr color space conversion formula is defined as Equation 2-10, 11, and 12 (ITU, 1995).

$$Y = 0.299R + 0.587G + 0.114B, \quad (2\text{-}10)$$

$$Cb = -0.172R - 0.339G + 0.511B + 128 \quad (2\text{-}11)$$

$$Cr = 0.511R - 0.428G - 0.083B + 128 \quad (2\text{-}12)$$

By substituting R, G, and B value with R', G' and B' value in Equation 3-12, Y', Cb', and Cr' component values were obtained. The components of YCbCr and Y'Cb'Cr' color space can range from 16 to 255.

Figure 2-15 and Figure 2-16 show the histogram of H', S', V' and Y', Cb', Cr' components. Unlike regular RGB images, images with the normalization of illumination had a similar intensity so that each class had less overlapping areas. In Figure 2-15, the H' component had distinctive variation between citrus and background objects including leaf, dead leaf, twig, soil and trees. Consequently, the H' component were used to classify the citrus from the background. However, in the S' component, each class was still overlapping most of other objects. The V' component is also another way of defining the amount of the light. Each of classes was processed by normalization of illumination so the classes had the similar V' component value.

Histograms of the Y', Cb' and Cr components are shown in Figure 2-16. The Y' value represents intensity which was defined in Equation 2-2. The intensity was normalized in the previous section, therefore, all classes had similar intensity values (Figure 2-16 (A)). In the Cb' component histogram (Figure 2-16 (B)), the high intensity area (highly saturated area) was distinguishable among other classes. In Figure 2-16 (C), the citrus class is distinguishable from tree, twig, dead leaf and soil classes.

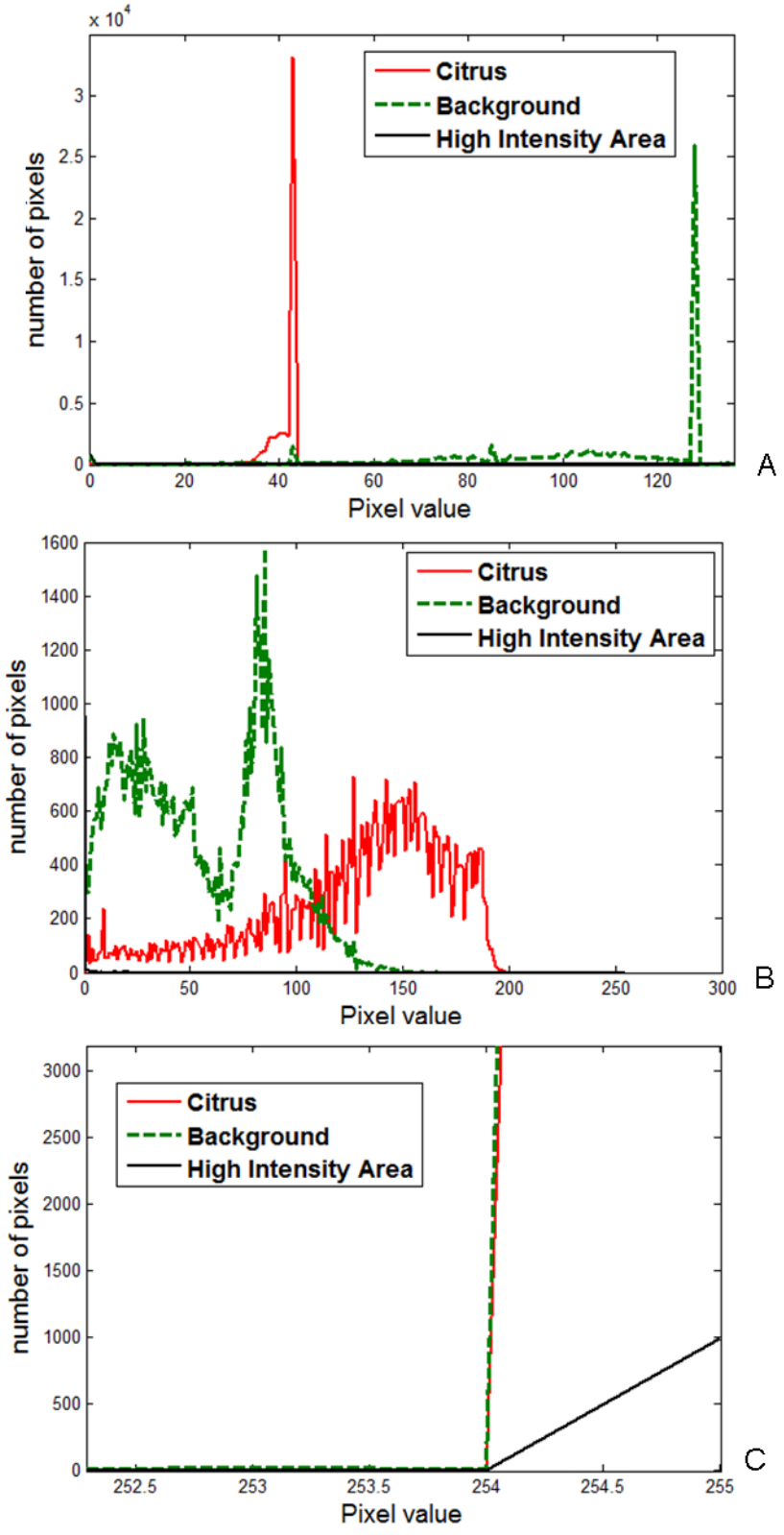

Figure 2-15. Histogram of H', S' and V' components (A, B and C, respectively).

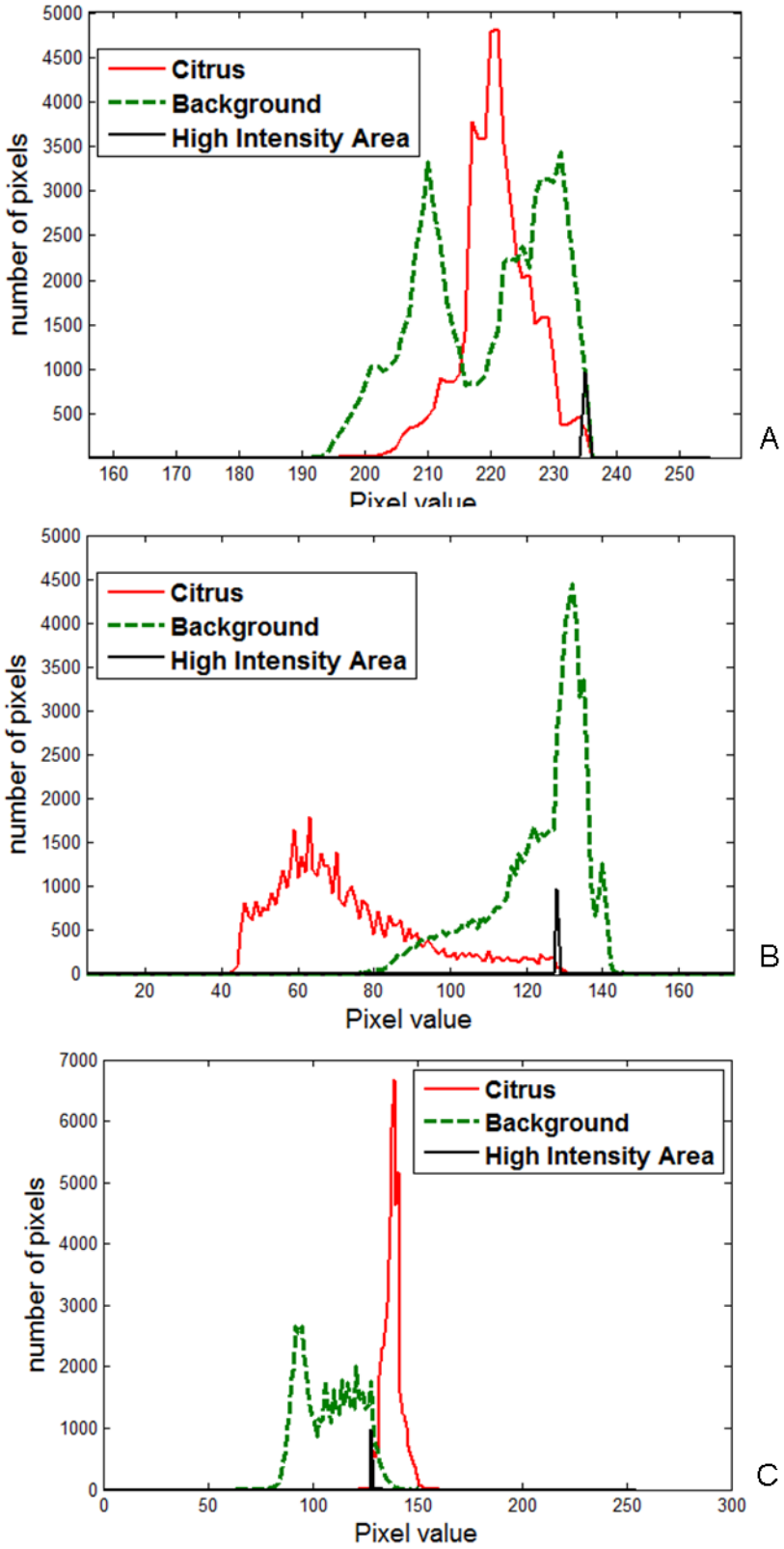

Figure 2-16. Histogram of Y', Cb', and Cr' components (A, B and C, respectively).

To sum up this section, the H' component along with the Cb' and Cr' color information were able to separate each class from others. Therefore, 3-color components information was chosen to compose the training information for a logistic regression classifier.

Classification

The color information demonstrated in previous section was used for training a classifier. This type of classifier is called memory based classifier (Atkeson et al., 1997). There are several kinds of well-known memory based classifier such as K-nearest neighborhood (KNN), Naïve Bayesian (Simple Bayesian) and a logistic regression classifier (Deng, 1998).

KNN classifier is known for overall good performance. However, it may yield a low accuracy near boundaries of classes since the classifier does not discriminate the different class near boundaries. Also, another reason for having a low accuracy is that the classifier is likely to be affected by data density in the boundary area.

Also, a naïve Bayesian classifier tends to have low accurate result since it is based on a strong assumption that data is a Gaussian distribution which is not suitable for most cases.

In the algorithm, a logistic regression classifier was used for separating citrus from background. A logistic regression classifier is straightforward and simple and it has a good ability for extrapolation. Figure 2-7 shows a simple model for logistic regression classification. The classifier gives classes (0 and 1) to input data based on the probability to belong to one of its categories. The probability is calculated by a function shown as solid grey line in Figure 2-17. To estimate the function, the logistic model in Equation 2-13 was used.

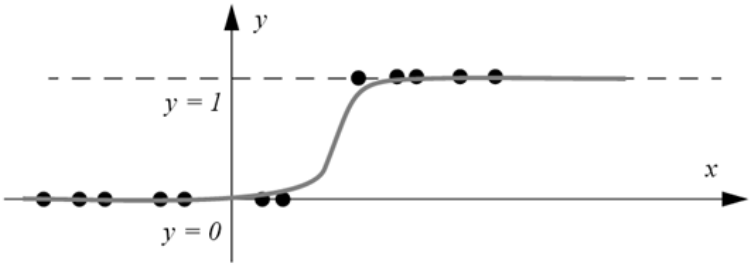

Figure 2-17 Simple logistic regression classifier model (Deng, 1998).

$$P = \frac{1}{1 + e^{(w^T x + w_0)}}, (P \in [0,1]) \tag{2-13}$$

where, x is an input data vector and w is a coefficient vector.

$$y = \begin{cases} 1 & with\ probablity\ P \\ 0 & with\ probability\ 1 - P \end{cases} \tag{2-14}$$

The coefficient of the function w=[w_1, w_2, w_3] and w_0 in Equation 2-13 was computed by fitting color values obtained from training data set in vector *x*. The vector *x* was constituted as in Equation 2-15.

$$\begin{gathered} \mathrm{x} = [x_1, x_2, x_3] \\ \text{where } x_1 = H' \text{ component value,} \\ x_2 = \mathrm{Cb}' \text{ component value,} \\ x_3 = \mathrm{Cr}' \text{ component value.} \end{gathered} \tag{2-15}$$

The estimated function was used to classify the pixels in the images. Figure 2-18 (A) shows an original image. The logistic regression classifier processed each pixel in the image and the output value from the classification was assigned in every pixel. In other words, the probability that the pixel belongs to the citrus class was given in each pixel. The confidence level was set to 0.95 so that the classifier assigned citrus class if the pixel has the probability equal or greater than 0.95. Other pixels which had the probability less than 0.95 were classified as background objects.

A

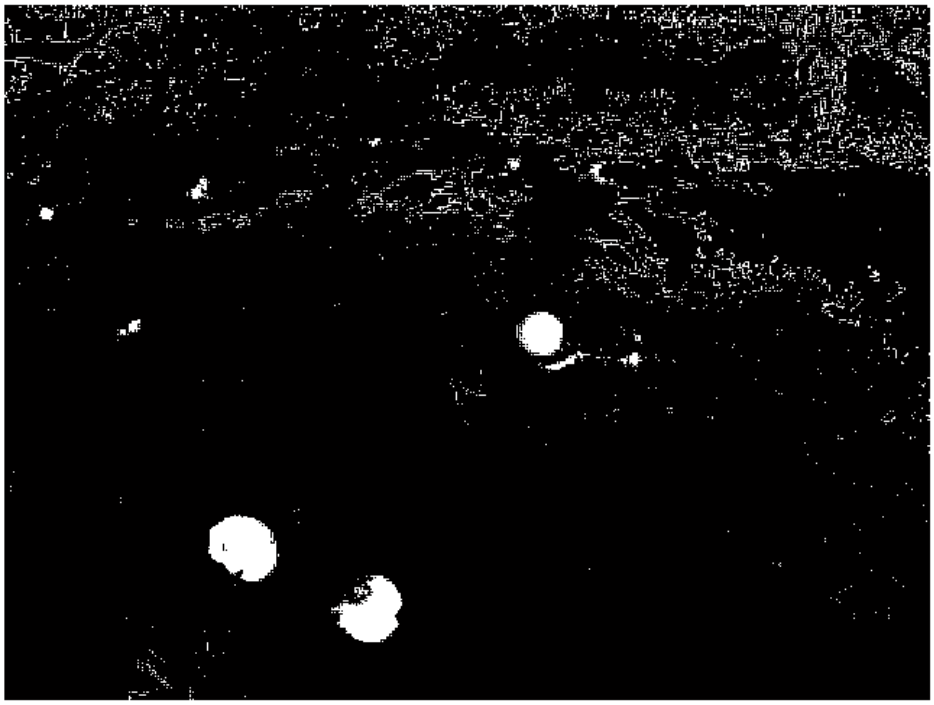

B

Figure 2-18. Example of classification result. A) Original Image. B) Binary image after the classification using logistic regression.

Figure 2-18 (B) shows the result image after the logistic classification and most of the citrus pixels were classified as citrus class compared to the original image.

However, not only citrus pixels were detected but also pixels of leaf, tree and twig which had high intensity were also classified as citrus.

Citrus Classification Using Entropy Texture Analysis

Using entropy texture analysis, only citrus was extracted. Entropy of a pixel in the image represented randomness of the pixel with its neighborhood. For example, if the image was pure black color with no contrasting objects, every pixel had very low entropy. However, if there were white objects in the black background which have heavy contrast, boundary pixels of the objects would have high entropy values. In Figure 2-18 (B), the citrus had solid boundaries so it had great contrast to the background. However, noise pixels were scattered so its texture did not contain significant contrast. With this features, the entropy filter was applied to analyze the texture of objects. The entropy of pixel '*x*' is defined as in Equation 2-16.

$$\text{Entropy} = \text{E}[\log_2 P(X)] = -\sum_i P_i \log_2 P_i \,, \qquad \text{(2-16)}$$

where xi is i-th neighborhood of X,
and $P_i = \Pr(X = xi)$.

The entropy value of every pixel in the images was calculated using the Equation 2-16. The result image is shown in Figure 2-19 which visualized the entropy values. The brighter pixel had higher entropy while darker pixels had low entropy. After applying filter, the image had only pixels which had the entropy value equal or greater than 0.95. Figure 2-20 shows result after the filter and morphological operations such as filling holes inside of citrus pixels and remove small noise objects.

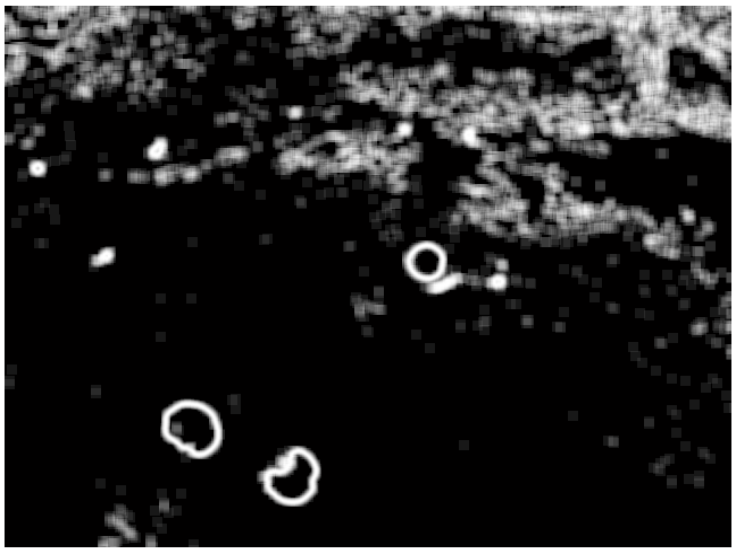

Figure 2-19. Visualization of entropy value. Brighter pixel represents the greater value.

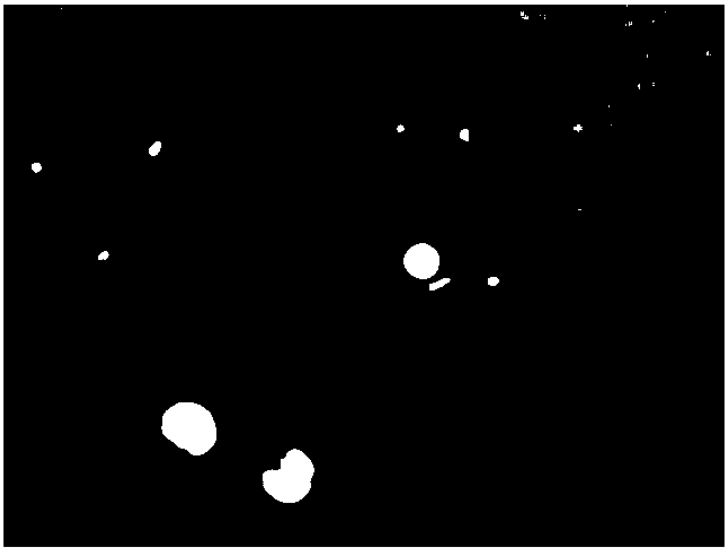

Figure 2-20. Morphological operations after entropy filter. Filling holes and removing small objects.

Counting and Mass Estimation

After detecting the citrus fruit, count and mass were estimated using least square circle fitting. Consequently, the number of fitted circle became the count of detected citrus fruit. The circle fitting method provided position and diameter of detected citrus which were important information to estimate the mass. The least square circle fitting was based on a circle equation shown in Equation 2-17.

$$\hat{x}^2 + \hat{y}^2 + a_1\hat{x} + a_2\hat{y} + a_3 = 0, \quad (2\text{-}17)$$

where, $\hat{x}$: coordinate in column axis of boundary pixels of detected fruit,
$\hat{y}$: coordinate in row axis of boundary pixels of detected fruit.

With the coordinate of boundary pixels of detected citrus, the coefficients (a_1, a_2 and a_3) which minimized the norm of the Equation 2-17 were estimated. In the algorithm, 2-norm was used to estimate the coefficients and it is defined as in Equation 2-18.

$$\|R\|_2 = \sqrt[2]{\sum |r_i|^2} \quad (2\text{-}18)$$

Conversion to the mass of detected citrus involved a couple of steps. Firstly, the position and diameter of detected citrus fruit that were calculated from least square circle fitting were converted into actual size of citrus. In images, objects were bigger in close distance while further objects were smaller. For accurate estimation of the actual size, the position was used as well as the diameter. Bilinear relationship between the actual size of citrus, the position and the diameter in images were modeled from a calibration data set. In Figure 2-21 (B), three different sizes (6.4, 7.6 and 10.2 cm) of the Styrofoam ball were measured their diameter in pixel according to their position in the image. The camera angle and height were fixed at the same angle and height with the field experiment. A conversion table was created to find its actual size using the diameter in pixel and position in the image.


A

B

Figure 2-21. Calibration images. A) Measuring the relationship between the diameter and the mass of actual fruit. B) Measuring the diameter in pixel count according to the size (6.4, 7.6 and 10.2 cm)

For the second step, the estimated actual size of the citrus was converted into the mass. This step involved another calibration data set between the diameter and the mass of the citrus. Figure 2-21 shows the citrus that were used in mass and diameter measurements. A total of 43 citrus was measured its mass and diameter. Two kinds of diameter were measured: major (long) and minor (short). Then, the average of the two diameters was calculated. The relationship between mass and the average diameter was estimated by second order polynomial curve fitting.

To sum up, the number of circles were considered as fruit count after fitting circles on detected citrus. The diameter and the position were converted to the actual size of citrus. Then the actual size of citrus was converted to mass of fruit in the images.

CHAPTER 3
RESULT AND DISCUSSION

Firstly, result for measurement of the actual diameter of citrus and the diameter in images are shown in Table 3-1. Three different sizes of balls (6.4, 7.6, and 10.2 cm) were measured its diameter in images according to its position (row number) in images.

Table 3-1. Measurement of diameter in number of pixels for three different sizes of white balls.

Actual size (cm)	Row number In the image	Radius (pixel)	Diameter (pixel)
6.4	223	15.5	30.9
6.4	95	9.9	19.8
6.4	167	12.6	25.1
6.4	73	8.6	17.2
6.4	124	11.7	23.4
7.6	218	18.5	36.9
7.6	161	14.5	29.0
7.6	94	10.6	21.2
7.6	124	12.3	24.7
7.6	73	9.7	19.3
10.2	212	24.9	49.9
10.2	158	19.9	39.7
10.2	91	14.1	28.2
10.2	121	16.6	33.2
10.2	71	12.1	24.2

The row number ranged from 1th (the farthest row from the camera) to 480th (the closest row to the camera). At same distance from the camera, citrus size in images increased linearly as the size of ball increased. Additionally, for the same size of balls, the diameter of citrus in images had linear decreasing relationship with the distance from the camera. Based on the measurement in Table 3-1, linear interpolation and extrapolation were applied to estimate the bilinear relationship between the diameter and position in images and the actual size of the citrus fruit. Table 3-2 shows a part of

conversion table which were created to find actual size of the detected citrus. With the table, if the diameter and the position were specified, the actual size of diameter in cm was calculated. For example, if the detected citrus was located in 160th row and diameter in an image was 29.0 pixels, then the actual size of the detected fruit would be equal to 7.6 cm.

Table 3-2. 2D look-up table (bilinear) for estimating actual size of detected fruit.

Size/ Row No.	6.4 cm	7.6 cm	10.2 cm
40	12.9	16.2	17.5
80	18.1	20.0	25.6
120	22.9	24.3	32.7
160	25.1	29.0	39.7
200	29.2	34.6	46.8
240	33.2	40.1	54.0
280	37.3	45.7	61.1
320	41.3	51.3	68.3
360	45.4	56.9	75.4
400	49.4	62.5	82.5
440	53.5	68.1	89.7
480	57.5	73.7	96.8

After estimating the actual size of fruit, the mass was estimated. Table 3-3 shows measured average diameter and mass of 43 citrus in a calibration set and its estimated mass. The estimated mass was calculated by regression Equation 3-1.

Table 3-3. Measured diameter (cm), actual mass (g) and estimated value

Average Diameter (cm)	Actual Mass (g)	Estimated Mass (g)
5.53	152	117.8
5.97	121	130.9
6.12	121	137.1
6.14	131	138.0
6.23	135	142.2
6.25	140	143.2
6.30	142	145.8
6.38	146	149.6
6.38	141	149.6
6.50	155	156.5

Table 3-3 Continued.

Average Diameter (cm)	Actual Mass (g)	Estimated Mass (g)
6.75	165	172.2
6.75	173	172.2
6.75	186	172.2
6.88	170	181.0
6.88	186	181.0
6.88	187	181.0
6.88	173	181.0
6.88	175	181.0
7.13	187	200.2
7.13	200	200.2
7.13	202	200.2
7.25	203	210.8
7.25	229	210.8
7.25	218	210.8
7.38	229	221.9
7.50	243	233.6
7.50	230	233.6
7.50	245	233.6
7.63	241	245.8
7.63	240	245.8
7.63	258	245.8
7.75	248	258.7
7.75	264	258.7
7.75	254	258.7
7.75	264	258.7
8.00	287	286.2
8.00	300	286.2
8.13	310	300.9
8.13	315	300.9
8.38	316	331.9
8.50	350	348.3
8.75	363	382.9
8.75	385	382.9

$$\mathrm{Mass}(d) = 18.88 * d^2 - 187.3 * d + 576.3, \quad (3\text{-}1)$$

where, *d* is the average fruit diameter.

Equation 3-1 shows a relationship between actual mass and average of actual diameter of citrus. The relationsip was estimated by second order curve fitting. Figure 3-1 shows the graph of the fitted curve and data points from Table 3-3. Scattered dots represents the actual fruit diameter and the mass and solid blue line shows the fitted

curve. For the curve fitting, the coefficient of determination(R^2) was 0.94 between the average diameter and the mass.

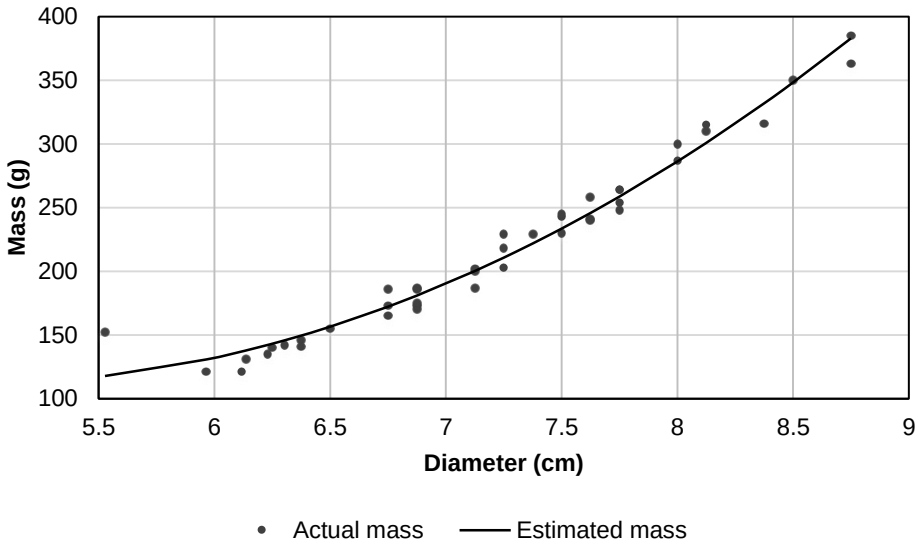

Figure 3-1. Regression of the size and the mass of actual citrus measurements.

Figure 3-2 shows an example of fruit count and mass estimation. Each detected citrus was marked as a red circle in Figure 3-2 (B). A total number of citrus was eight in this image because the algorithm was programmed to ignore unhealthy or defected citrus fruit. The estimated mass was 1530.5 g.

The performance of the algorithm was analyzed by two criteria accuracy and false positives. Firstly, the accuracy which represents an ability of the algorithm to detect citrus fruit without any missed fruit was analyzed by comparing actual citrus count by manual counting and citrus count which were correctly identified by the machine vision algorithm. Missed citrus fruit which represents object existing in the image but failed to be counted by the algorithm were counted as well.

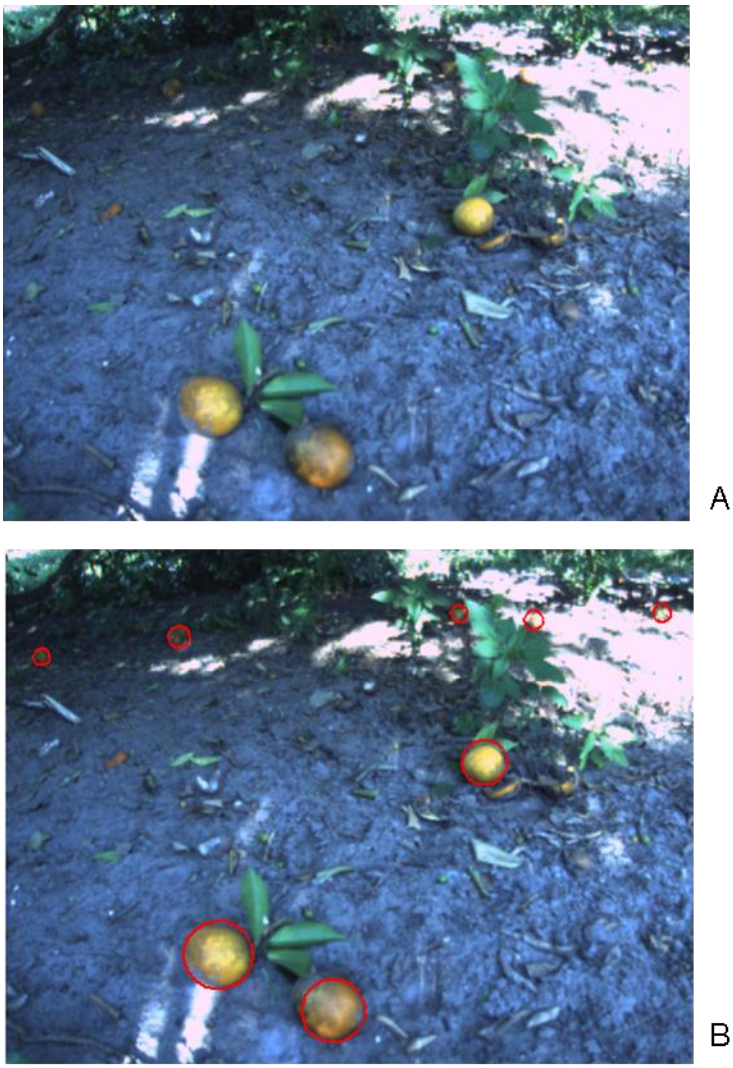

Figure 3-2. Final result example. A) Original image. B) Final result. The number of count: 8, the mass: 1530.5 g

The accuracy from seven trials in skirted canopy in Lykes grove is shown in Table 3-4. A total of 1470 images was collected and 1352 images were used as the validation set. Trial 1 had the most number of actual fruit drop which was 1650 citrus while trial 3 had the least actual fruit drop which was 430. The mean of the actual fruit drop for seven trials was 1019. The accuracy is shown in fifth and sixth columns. The highest accuracy was in trial 6 which was 89.5 percent and the missed fruit were 10.5 percent. This was because the images in trial 6 were clearer so it had a great contrast

compared to the images in other trials. However, trial 2 had the least accuracy which was 59.3 percent. The source of error was from that the images were dark and unclear which contained less color variation between citrus and background. Also, the citrus in the trial 2 were located further than in other trials so some of the citrus was too small to be detected. The average accuracy in skirted canopy was 74.8 percent.

Table 3-4. Performance of algorithm for accuracy and estimated mass (skirted canopy, Lykes grove).

	Fruit Count by Manual Counting	Correctly Identified Fruit by Algorithm	Missed Fruit	Correctly Identified Fruit by Algorithm (%)	Missed Fruit (%)	Estimated Mass (kg)
Trial1	1650	1322	328	80.1	19.9	316.5
Trial2	1448	859	589	59.3	40.7	282.3
Trial3	430	330	100	76.7	23.3	142.0
Trial4	1102	784	318	71.1	28.9	179.0
Trial5	885	707	178	79.9	20.1	201.5
Trial6	618	553	65	89.5	10.5	157.2
Trial7	999	782	217	78.3	21.7	224.8
Sum	7132	5337	1795	-	-	1503.2
Mean	1018.9	762.4	256.4	74.8	25.2	214.7

For the mass estimation, trial 1 had the highest mass which was 316.4 kg and trial 3 had the least mass which was 141.9 kg. This result corresponded to the drop counts which were also the highest value in trial1 and the least value in trial 3. However, the mass in trial 4 was estimated less than trial 5 although the citrus count by the algorithm was higher in trial 4. This error was from a smaller size of the fruit in images. The images in trial 4 were taken further than in trial 5 so that the mass of the citrus was underestimated.

Another performance analysis was for false positives. The false positive object is incorrectly detected background objects as citrus. False positive error was calculated by

dividing false positive count by citrus fruit count by algorithm. Fourth and fifth columns in Table 3-5 show false positive count and its percentage. Most of false positives were from soil and leaf pixels in high illumination areas. These pixels had bright and yellowish colors which was similar with citrus. The highest error was in trial 3 because the images had unclear distinction between unhealthy and healthy citrus in dark areas. While the algorithm was counted as healthy fruit, manual counting considered them as unhealthy fruit.

Table 3-5. Performance analysis for false positives (skirted canopy, Lykes grove).

	Citrus Fruit Count by Algorithm	Correctly Identified Fruit by Algorithm	False Positive Count	False Positive (%)
Trial1	1466	1322	144	9.8
Trial2	881	859	22	2.5
Trial3	473	330	143	30.2
Trial4	815	784	31	3.8
Trial5	766	707	59	7.7
Trial6	652	553	99	15.2
Trial7	932	782	150	16.1
Sum	5985	5337	648	-
Mean	855	762.4	92.6	10.8

Also, performance of the algorithm for un-skirted canopy images from Duda grove was analyzed. Accuracy and estimated mass are shown in Table 3-6. The accuracy was 76.4 percent in un-skirted canopy which was similar with the result from skirted canopy.

Table 3-6. Performance analysis for accuracy and estimated mass (un-skirted canopy, Duda grove).

Number of Fruit by Manual Counting	Correctly Identified Fruit by Algorithm	Missed Fruit	Correctly Identified Fruit by Algorithm (%)	Missed Fruit (%)	Estimated Mass (kg)
3580	2735	845	76.4	23.6	835.7

The false positives from un-skirted canopy shown in Table 3-7 was relatively higher than in Lykes grove (average 10.8 percent). This is because many images included more occluded citrus fruit from un-skirted canopy.

Table 3-7. Performance analysis for ability to avoid false positive error (un-skirted canopy, Duda grove).

Number of Fruit Counted by Algorithm	Correctly Identified Fruit by Algorithm	False Positive Count	False Positive (%)
3294	2735	559	17.0

The different result might be derived if the images contain more extreme illumination conditions. By the normalization of illumination in the machine vision algorithm, most of the varying illumination effect was compensated. However, over-exposure images or excessively dark images might not be normalized successfully. These extreme illumination conditions may lower the accuracy and cause higher false positives. Therefore, staying within certain range of illumination is important for reliable normalization of illumination.

Also, in the experiments, canopy shakers and catch frames were used for mechanical harvesting so the fruit drop from the mechanical harvesting was not piled up. However, another type of mechanical harvester, a trunk shaker, causes fruit drop to be piled in multiple layers on the ground. In that situation, the machine vision algorithm would yield low performance to detect all of the citrus, especially in a bottom layer. Therefore, different estimation process needs to be developed for the trunk shakers.

These accuracy and false positives can be improved by adopting correction factors based on conditions of grove, trees, and images which will be studied in future works.

Also, the experiment result shows that each area in citrus groves had different fruit drop. The spatial variation map of fruit drop was created using a map with DGPS coordinates obtained during image acquisition. The mass of the fruit drop was converted to mass per unit area. Area of each image was calculated by multiplying distance between locations where images were taken by average row spacing in citrus grove. The distance between images was computed from DGPS coordinates. Figure 3-3 and Figure 3-5 show full view of citrus drop map. Entire rows of data points were shown in the maps. Figure 3-4 and Figure 3-6 represents zoomed view of the fruit drop maps. In zoomed view, each data point was more distinguishable so that readers can recognize the variation of fruit drop. The possible reason of the variation of each point is that each area had different spatial variability factors such as canopy size, nutrient level, soil pH, and disease. Among those factors, spraying CMNP caused substantial fruit drops. In Duda grove, citrus drop was much higher than in Lykes grove even though the images in Duda grove were acquired before harvesting while the images in Lykes grove were acquired after mechanical harvesting. The most suspected reason was that the trees in Duda grove were sprayed with CMNP several days before image acquisition so the CMNP allowed trees to drop its fruit before harvesting. However, impact of the CMNP which was sprayed during past couple of years was not shown specifically. Trial 6 in Lykes grove was sprayed with CMNP during past couple of years, however fruit drop count was lower compared to other non-sprayed area in past years.

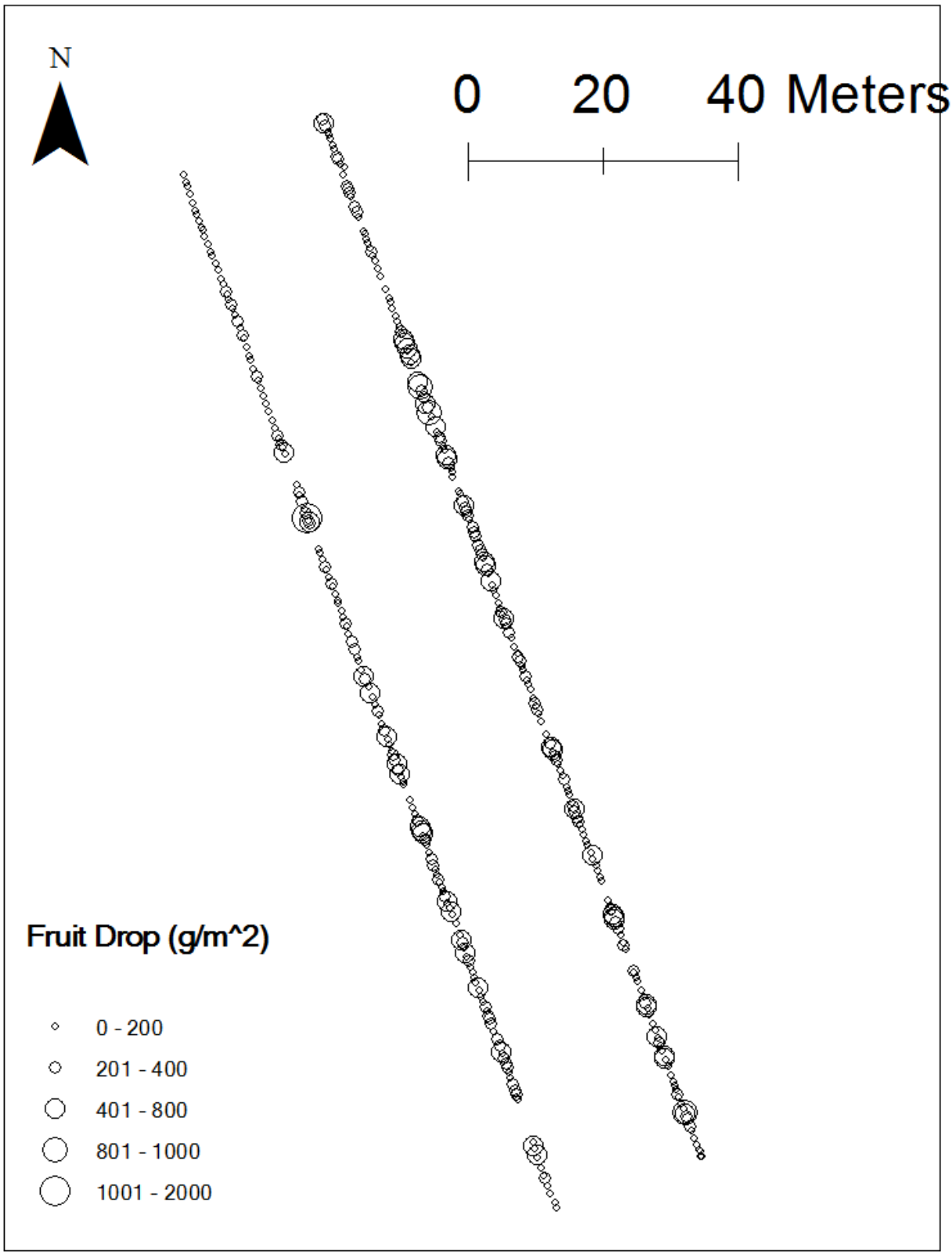

Figure 3-3. Full view of fruit drop map in Lykes grove.

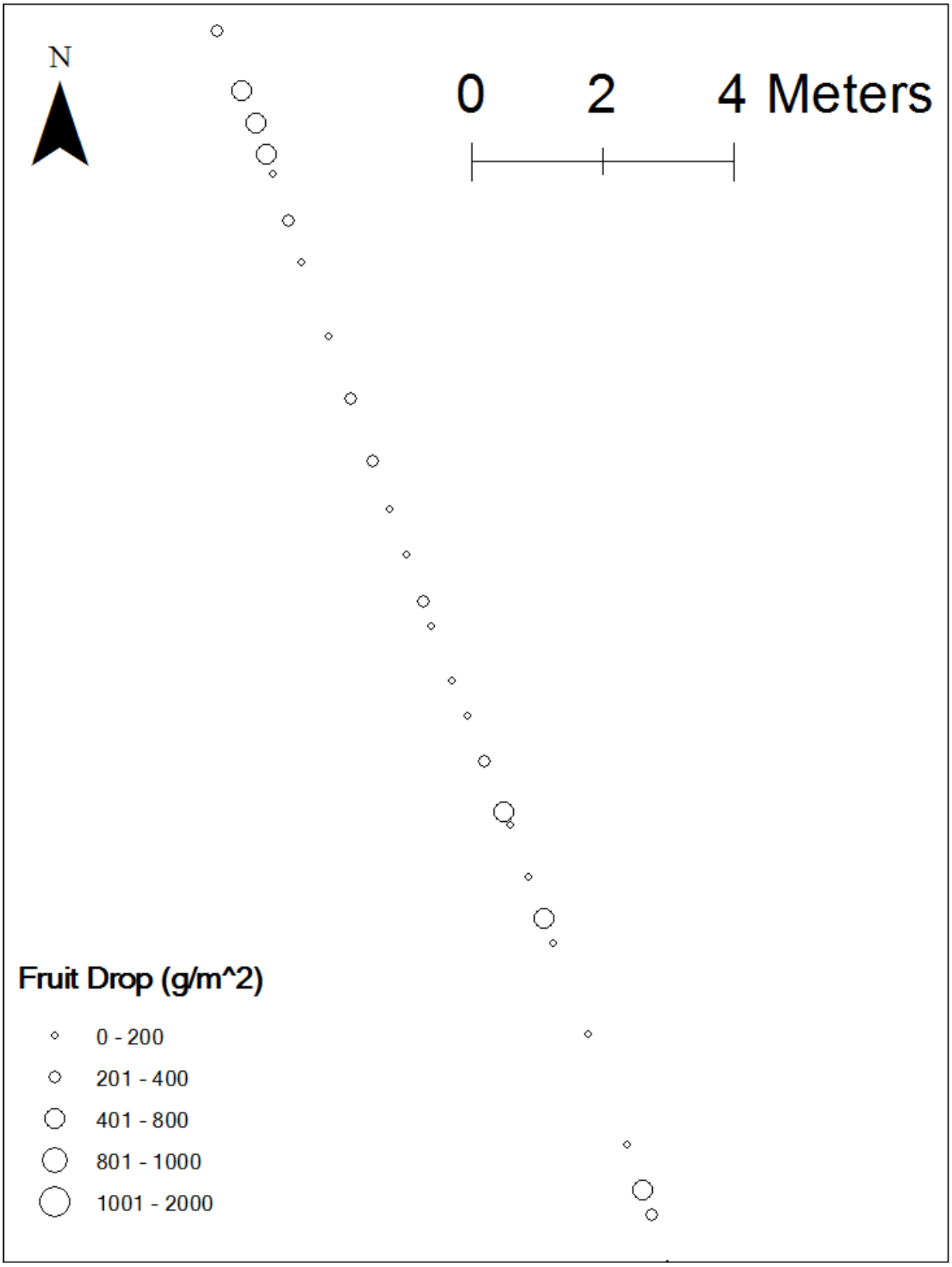

Figure 3-4. Zoomed view of fruit drop map in Lykes grove.

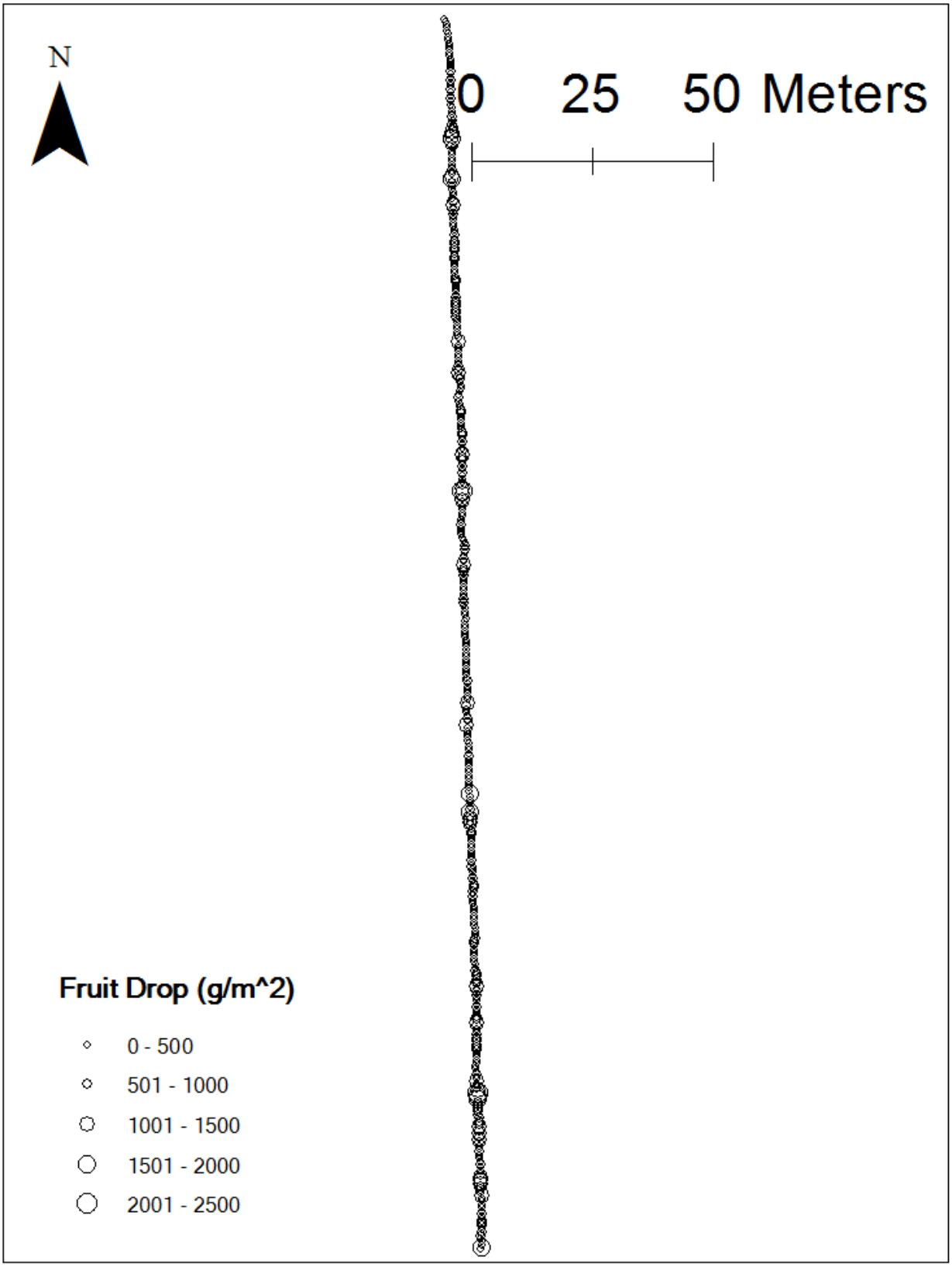

Figure 3-5. Full view of fruit drop map in Duda grove

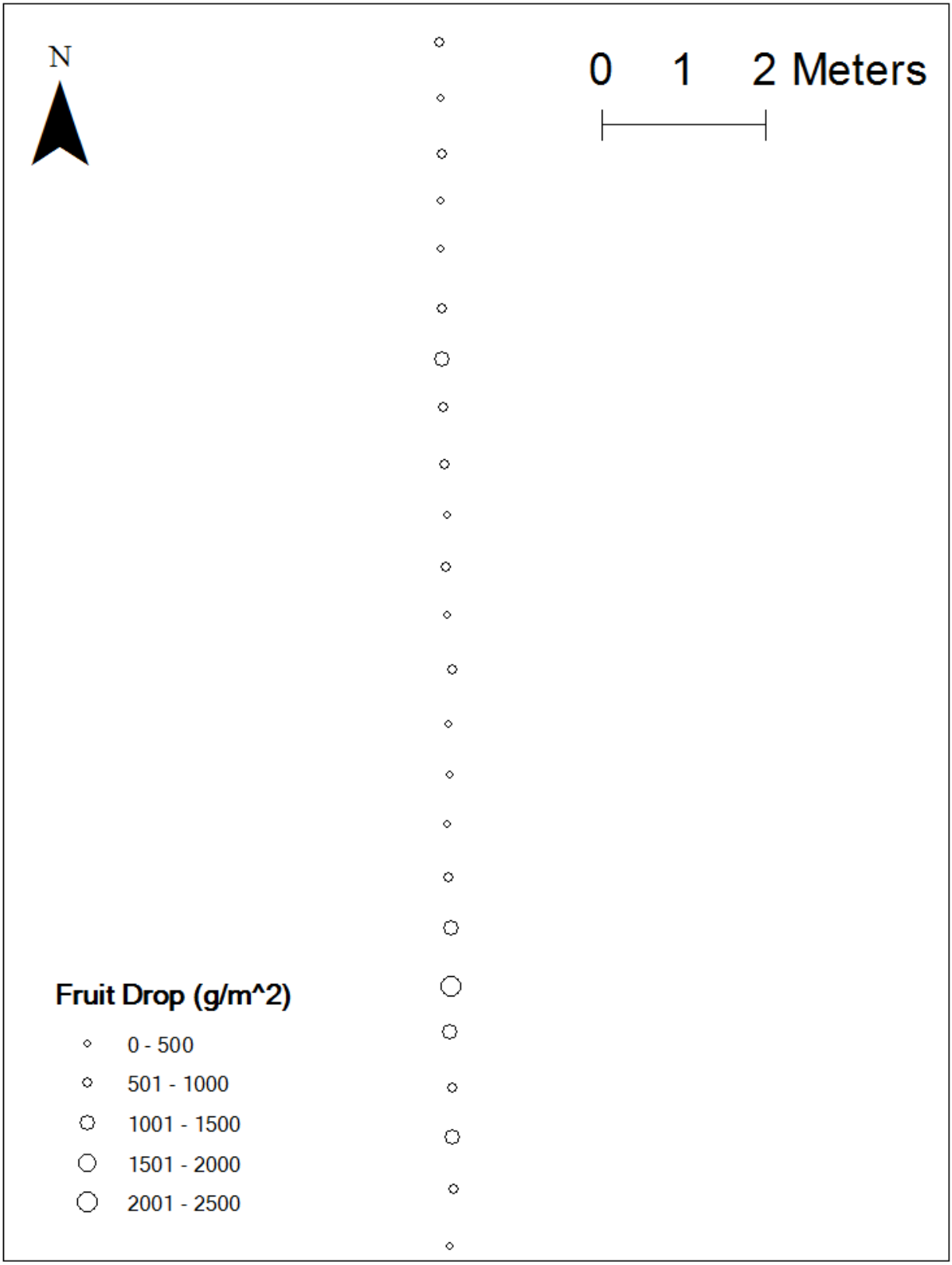

Figure 3-6. Zoomed view of fruit drop map in Duda grove.

CHAPTER 4
CONCLUSION

The rugged hardware system was developed for outdoor commercial citrus grove. The system included two cameras with a microprocessor, an encoder, a DGPS receiver, and mounting frames. The cameras were installed on moving vehicle and triggered by the encoder to measure distance between the positions where the images were taken. This method enabled to take images automatically while moving with a vehicle and avoiding overlapping areas between images. Taking images on the moving vehicle significantly reduced image acquisition time. After the image acquisition, DGPS coordinates were obtained to create geo-referenced citrus fruit drop map.

The machine vision algorithm included the normalization of illumination, citrus detection by a logistic regression classifier, least square circle fitting for estimating count and mass of citrus fruit drop. The normalization of illumination reduced the effect of the varying illumination conditions. After the normalization, the color space conversion was conducted in H'S'V' and Y'Cb'Cr color spaces. Then, a logistic regression classifier assigned object to the citrus class based on the similarity of colors. Texture filter using entropy successfully removed background objects which were incorrectly detected as the citrus. Detected citrus fruit was fitted to a circle using least square circle fitting method which calculated position and diameter of citrus. With the calibration data, actual size and mass of the citrus fruit was estimated.

Field experiments were conducted in un-skirted canopy in Duda & Sons grove (Immokalee, FL) and skirted canopy in Lykes Bros. Inc. grove (Ft. Basinger, FL). The citrus fruit dropped on the ground during the harvesting season was considered in the experiments.

The performance of the algorithm was analyzed using accuracy and false positives. The highest accuracy was 89.5 percent while the lowest accuracy was 59 percent in skirted canopy and 76.4 percent in un-skirted canopy. For the false positive error, percentage of false positive fruit also varied between the trial set while the highest error was 30 percent and the lowest error was 2.6 percent in the skirted canopy, and 17.0 percent in the un-skirted canopy.

The performance of the algorithm can be improved by alternative imaging devices. In the experiments, two cameras were used and each camera covered entire area under canopy at a time to expedite image acquisition and processing. Consequently, field of view was wide so that the citrus in the images was small. Small objects in the images caused missed fruit because it did not contain enough amount of information to be detected. This problem can be improved using higher resolution camera or using multiple cameras so the objects contain enough information such as color and shape. Also, image acquisition time can be improved by using a video camera. Two cameras were triggered by encoder pulses in order to acquire images. However, this method increased unnecessary image acquisition time from encoder pulse detection, counting and triggering the cameras. Using a video camera and image stitching techniques, image acquisition process can be simplified.

By increasing image quality and number of cameras, the machine vision algorithm can be modified for advanced applications. Those future works will be immature citrus fruit drop detection during mechanical harvesting and early yield estimation. Immature citrus fruit drop detection during mechanical harvesting will ascertain optimal speed of mechanical harvester so it would reduce future yield loss.

Also, modifying image acquisition system to acquire images of an entire tree will enable early estimation of citrus production.

LIST OF REFERENCES

Alexander, H. 2006. Handbook of machine vision. Wiley-VCH.

Atkeson, C. G., A. W. Moore, and S. Schaal. 1997. Locally weighted learning. *Artificial Intelligence Review* 11(1-5): 11-73.

Annamalai, P., and W. S. Lee. 2003. Citrus yield mapping system using machine vision. ASAE Meeting Paper No. 031002. St. Joseph, Mich.: ASAE.

Annamalai, P., and W. S. Lee, T. F. Burks. 2004. Color vision system for estimating citrus yield in real-time, ASAE/CSAE Meeting Paper No. 043054. St. Joseph, Mich.: ASAE.

Chi, Y., and P. P. Ling. 2004. Fast fruit identification for robotic tomato picker. ASAE/CSAE Meeting Paper No. 043083. St. Joseph, Mich.: ASAE.

Chinchuluun, R., W. S. Lee, and R. Ehsani. 2009. Machine vision system for determining citrus count and size on a canopy shake and catch harvester. Applied engineering in agriculture 25: 451-458.

Deng, K. 1998. Omega: on-line memory-based general purpose system classifier. PhD diss. Pittsburgh, PA: Carnegie Mellon University, School of Computer Science.

Gonzalez, R. C., and R. E. Woods. 2008. *Digital Image Processing Third Edition*. Upper Saddle River, New Jersey: Prentice Hall.

ITU. 1995. Studio encoding parameters of digital television for standard 4:3 and widescreen 16:9 aspect ratios. Available at: http://www.itu.int/dms_pubrec/itu-r/rec/bt/R-REC-BT.601-5-199510-S!!PDF-E.pdf. Accessed 08 May 2013

John Deere Company. 2010. T*he Precision-Farming Guide for Agriculturists*. Moline, Illinois: John Deere Publishing.

Kurtulmus, F., W. S. Lee, and A. Vardar. 2011. Green citrus detection using ‘eigenfruit’, color and circular Gabor texture features under natural outdoor conditions. *Computers and Electronics in Agriculture* 78: 140-149.

Li, H., W. S. Lee, K. Wang, R. Ehsani, and C. Yang. 2013. ‘Extended spectral angle mapping (ESAM)’ for citrus greening disease detection using airborne hyperspectral imaging. Precision Agriculture Published online. Available at: http://link.springer.com/article/10.1007%2Fs11119-013-9325-6.

Ling, P., R. Ehsani, K. Ting, Y. Chi, N. Ramalingam, M. Klingman, and C. Draper. 2004. Sensing and end-effector for a robotic tomato harvester, ASAE/CSAE Meeting Paper No. 043088. St. Joseph, Mich.: ASAE.

Okamoto, H., and W. S. Lee. 2009. Green citrus detection using hyperspectral imaging, *Computers and electronics in Agriculture* 66: 201-208.

Patel, H. N., R. K. Jain, and M. V. Joshi. 2012. Automatic segmentation and yield measurement of fruit using shape analysis. *International Journal of Computer Applications* 45(7): 19-24.

Pourreza, A. W. S. Lee, E. Raveh, Y. Hong, and H. Kim. 2013. Identification of citrus greening disease using a visible band image analysis. ASABE Meeting Paper No. 131591910. St. Joseph, Mich.: ASABE.

Shin, J. S., W. S. Lee, and R. Ehsani. 2012. Postharvest citrus mass and size estimation using a logistic classification model and a watershed algorithm. *Biosystems Engineering* 113(1): 42-53.

Stanjnko, D., M. Lakota, and M. Hocevar. 2004. Estimation of number and diameter of apple fruits in an orchard during the growing season by thermal imaging. Computers and Electronics in Agr. 42: 31-42.

USDA. 2013. Citrus: World market and trade. Washington, D.C.: USDA Foreign Agricultural Service, Citrus: World market and trade, Available at: http://www.fas.usda.gov/psdonline/circulars/citrus.pdf. Accessed 01 August 2013.

USDA. 2012. Citrus October forecast. Washington, D.C.: USDA National Agricultural Statistics Service. Available at: http://www.nass.usda.gov/Statistics_by_State/Florida/Publications/Citrus/cit/2012-13/cit1012.pdf. Accessed 08 May 2013.

USDA. 2013. Citrus April forecast. Washington, D.C.: USDA National Agricultural Statistics Service. Available at: http://www.nass.usda.gov/Statistics_by_State/Florida/Publications/Citrus/cit/2012-13/cit0413.pdf. Accessed 08 May 2013.

Yang, C., W. S. Lee, and J. G. Williamson. 2012. Classification of blueberry fruit and leaves based on spectral signatures. Biosystems Engineering 113(4): 351–362.

Yang, L., J. Dickinson, Q. Wu, and S. Lang. 2007. A fruit recognition method for automatic harvesting. *14th International Conference on Mechatronics and Machine Vision in Practice,* 152-157. Washington, D.C.: IEEE.

Zhao, J., J. Tow, and J. Katupitiya. 2005. On-tree fruit recognition using texture properties and color data. *2005 IEEE/RSJ International Conference on Intelligent Robots and Systems*, 263-268. Washington, D.C.: IEEE.

BIOGRAPHICAL SKETCH

Daeun Choi is a master student and research assistant in Precision Agriculture Lab in University of Florida. She received bachelor's degrees in bio-mechatronic engineering and economics from Sungkyunkwan University, Seoul, Korea in 2011. After finishing undergraduate programs, she moved to the United States to pursue higher education in University of Florida, Gainesville, FL, in 2011. She is completing master's programs in department of agricultural and biological engineering. Currently, her research is focused on developing machine vision system for agricultural applications.